

Controlling $\langle \hat{S}^2 \rangle$ in Broken-symmetry Density Functional Theory Calculations via Constrained Optimization

Jerónimo Lira^{a)} and Juan E. Peralta^{b)}

*Department of Physics, Central Michigan University, Mount Pleasant,
Michigan 48859, USA*

Accurate determination of magnetic exchange coupling constants (J) from density functional theory (DFT) remains challenging, particularly for open-shell systems where broken-symmetry (BS) solutions suffer from spurious spin contamination that systematically exaggerates J values. Several methods have been proposed to address this problem by adjusting the mapping scheme from the DFT energies to the Heisenberg-Dirac-van Vleck effective spin Hamiltonian energies. In this work, we explore a different route by imposing a constraint to the DFT energy that enforces a target value of the spin-squared expectation, $\langle \hat{S}^2 \rangle$, using a Lagrange multiplier approach. By explicitly controlling the spin character of the electronic state, the method attempts to overcome limitations of standard BS calculations to describe magnetic interactions. As part of the theoretical formulation, we derive analytical expressions for the gradient of the spin-squared expectation value with respect to the spin-resolved density matrices, which are required for the practical implementation of the constraint within a generalized Kohn-Sham scheme. These expressions are general to any single-determinant method and remain valid for arbitrary spin states. We apply the spin-constrained approach to the calculation of J couplings and compare with three energy-difference-based schemes for a set of representative systems, including H_2He , H_3He_3 arranged in an equilateral triangle, and a bis(μ -hydroxo) Cu(II) complex. Across all cases, the constrained formulation yields systematically lower and more consistent exchange couplings across different density functional approximations. This work establishes a robust and general route for incorporating spin-state constraints into DFT-based studies of magnetic exchange interactions.

^{a)}lirap1j@cmich.edu

^{b)}peral1j@cmich.edu

I. INTRODUCTION

Calculations based on density functional theory (DFT) have become indispensable in electronic-structure, providing a pragmatic balance between accuracy and computational cost, enabling the investigation of large systems that are often prohibitively expensive to treat with high-level post-Hartree–Fock methods, such as coupled-cluster theory or configuration interaction. The Hohenberg–Kohn theorems provide a rigorous theoretical foundation for DFT by establishing that the ground-state energy is a functional of the electron density¹. The Kohn–Sham (KS) formalism offers a computationally tractable realization of this framework by introducing an auxiliary non-interacting reference system that reproduces the exact ground-state density of the interacting system². Collectively, these seminal developments have enabled quantitatively reliable predictions for a broad spectrum of molecular and condensed-phase systems at a fraction of the computational cost associated with wavefunction-based approaches. Commonly employed approximate functionals are subject to several well-documented deficiencies that compromise reliability in specific situations. The approximate nature of exchange–correlation functionals can give rise to self-interaction errors^{3,4}, erroneous localization or delocalization of charge^{5,6}, and incorrect spin-state energetics^{7,8}. Furthermore, conventional DFT is intrinsically formulated as a ground-state theory, rendering it poorly suited for a faithful description of electronically excited states or for imposing specific electronic configurations without additional methodological extensions or constraints^{9–13}. In systems whose electronic structure substantially deviates from the variationally preferred KS solution (such as those involving long-range charge transfer, localized magnetic moments, or pronounced symmetry breaking) approximate functionals may fail to reproduce the correct qualitative and quantitative physical behavior. These limitations underscore the need for theoretical frameworks that can systematically incorporate physically motivated constraints that explicitly target selected electronic properties.

Constrained density functional theory (CDFT) generalizes the conventional density functional framework by introducing explicit constraints on the electron density, typically expressed as functionals of the density. In doing so, CDFT enables access to electronic configurations that are not attainable within the standard, unconstrained KS formalism.^{14,15} The most commonly used strategy for enforcing such constraints relies on the incorporation of Lagrange multipliers into the variational procedure. This formulation permits the im-

sition of physically motivated conditions, such as fixed charges, spin moments, or orbital occupations, while remaining fully embedded within the DFT framework.¹⁴ As a consequence, CDFT has proven particularly useful for the description of charge-transfer states,¹⁶ localized excitations,¹⁷ and magnetic coupling mechanisms,^{18,19} among a variety of other phenomena.^{20–22} Crucially, CDFT preserves the computational efficiency characteristic of standard DFT while providing enhanced control over the electronic degrees of freedom. This additional flexibility broadens the range of systems and properties that can be described with quantitative accuracy.

One particular context in which the limitations of standard DFT become apparent is the broken-symmetry (BS) approach, which is extensively employed to model open-shell singlet states and magnetic coupling in systems exhibiting spin polarization.^{23,24} In BS DFT, the KS reference system is allowed to break spin symmetry in order to emulate a multi-configurational character within a single-determinant framework. Although this strategy enables access to low-spin (LS) solutions, the resulting states are not necessarily eigenfunctions of the total spin operator²⁵ and in general exhibit spin contamination, i.e., an undesired admixture of states with different total spin quantum numbers that complicates the physical interpretation of the computed results.^{26,27} In this setting, the expectation value of the total spin-squared operator, $\langle \hat{S}^2 \rangle$, is routinely used as a central diagnostic to quantify the extent of spin contamination in a given BS solution.^{26–28} Consequently, achieving accurate control over, or applying reliable corrections to, $\langle \hat{S}^2 \rangle$ is essential for a meaningful analysis of spin-dependent properties. This need has motivated the application of constrained CDFT and related methodologies to mitigate spin contamination and, consequently, improve the fidelity of spin-state descriptions within a DFT framework.^{26,29,30}

The BS approach is particularly useful for the determination of magnetic exchange coupling constants (J), which quantify the magnetic interactions between localized spin centers in polynuclear transition-metal complexes. These J couplings are commonly obtained from the energy differences between HS and BS solutions via the Heisenberg-Dirac-van Vleck (HDvV) Hamiltonian. Consequently, the accuracy of the BS state energy has a direct and critical influence on the predicted magnetic behavior. Because the energy separation between different spin states is typically small, even modest spin contamination in the BS solution (evidenced by deviations of $\langle \hat{S}^2 \rangle$ from its ideal symmetry-broken reference value) can introduce substantial errors into the calculated J constants. This spin contamina-

tion complicates the reliable approximation of BS solutions, motivating the development of various spin-decontamination schemes to address this problem.^{26,29,31} Alternative strategies include reformulating the DFT-to-Heisenberg mapping³² or using time-dependent DFT to access proper spin eigenstates.¹⁹ An early related approach was proposed by Löwdin, which consists in projecting the broken-symmetry determinant onto pure spin eigenstates using group-theoretical projection operators.³³ While Löwdin’s method guarantees that at least one projected state lies lower in energy than the original determinant, it requires numerical integration over the rotation group and becomes computationally demanding for large systems.

In addition, standard BS-DFT calculations are widely reported to overestimate the magnitude of J , particularly when using local and semi-local density functional approximations³⁴, further motivating approaches that enforce a more controlled spin character in the underlying BS reference. Thus, explicit control of $\langle \hat{S}^2 \rangle$ via CDFT methodologies becomes essential for obtaining dependable J values and for ensuring that the resulting magnetic couplings reflect the genuine electronic structure rather than artifacts arising from spin-state mixing. This work introduces such an approach within the generalized KS (GKS) formalism, wherein $\langle \hat{S}^2 \rangle$ is explicitly constrained during the self-consistent field (SCF) procedure via a Lagrange multiplier. By guiding the optimization of the spin-resolved density matrices toward target spin values, this method drives BS states toward the desired $\langle \hat{S}^2 \rangle$ and, to a lesser extent, reduces residual spin contamination in HS states.

It is important to remark that some BS solutions are intrinsically affected by spin contamination, and the aim of the present approach is not to remove this contamination entirely, but rather to control it in a physically motivated way. In the symmetry-broken limit³⁵, BS states correspond to well-defined linear combinations of spin eigenstates, which in turn yield characteristic target values of $\langle \hat{S}^2 \rangle$. In practical DFT calculations, however, these ideal values are seldom reproduced exactly. The deviations originate from the approximate nature of the exchange-correlation functionals, and in particular from self-interaction error, which favors excessive orbital delocalization and consequently alters the relative weights of the spin components.³⁶ As an illustrative case, consider the linear H–He–H molecule. The BS solution representing the open-shell singlet state corresponds, in the symmetry-broken limit, to a 50:50 admixture of singlet ($S = 0$, $\langle \hat{S}^2 \rangle = 0$) and triplet ($S = 1$, $\langle \hat{S}^2 \rangle = 2$) components, which leads to $\langle \hat{S}^2 \rangle = 1$. In practice, one typically obtains values slightly below

this ideal limit (e.g., $\langle \hat{S}^2 \rangle \approx 0.97$). Although such discrepancies may appear numerically small, they can induce non-negligible variations in the total energy. Since the evaluation of the exchange coupling constant J is highly sensitive to the energy difference between the HS and BS solutions, even minor deviations from the target $\langle \hat{S}^2 \rangle$ value can lead to substantial changes in the resulting J parameters. The capability to impose a consistent target $\langle \hat{S}^2 \rangle$ therefore offers a controlled and systematic strategy to mitigate these uncertainties.

The remainder of this article is organized as follows. Section II presents the theoretical framework and computational details of our CDFT implementation, including the variational formulation with a spin-squared constraint, analytical derivatives, and the exchange-coupling schemes used in this work. In Section III, we assess the performance of the method for H_2He , H_3He_3 , and the bis(μ -hydroxo) Cu(II) complex by comparing J values from unconstrained and constrained energies. Section IV summarizes our findings.

II. THEORY AND COMPUTATIONAL DETAILS

The ground-state DFT energy is obtained by minimizing an energy functional expressed in terms of the electron spin densities n^σ , where $\sigma = \alpha, \beta$ denotes the two possible spin projections in the collinear spin-polarization framework.^{37–39} The KS energy functional is written as:

$$E_{\text{DFT}}[n^\alpha, n^\beta] = \sum_a \left\langle \psi_a \left| -\frac{1}{2} \nabla^2 \right| \psi_a \right\rangle + E_H[n] + \int v(\mathbf{r}) n(\mathbf{r}) d^3\mathbf{r} + E_{\text{XC}}[n^\alpha, n^\beta], \quad (1)$$

where $n = n^\alpha + n^\beta$ is the total electron density, the first term in the r.h.s. of Eq 1 represents the kinetic energy of non-interacting electrons, $E_H[n]$ is the classical Coulomb energy (also known as Hartree energy), $v(\mathbf{r})$ is the external potential including the electron-nuclei interaction, and $E_{\text{XC}}[n^\alpha, n^\beta]$ is the exchange-correlation energy functional, which accounts for all the quantum mechanical effects beyond the classical electrostatics.

The constraint problem can be formulated through the Lagrangian formulation,

$$W[n^\alpha, n^\beta, \lambda] = E_{\text{DFT}}[n^\alpha, n^\beta] + \lambda \left(\sum_\sigma \int w^\sigma(\mathbf{r}) n^\sigma(\mathbf{r}) d^3\mathbf{r} - C \right), \quad (2)$$

where λ is the Lagrange multiplier, $w^\sigma(\mathbf{r})$ are prescribed weight functions defining the constrained quantity, and C is its target value. This Lagrangian is made stationary with respect

to the variational variables $n^\sigma(\mathbf{r})$ and λ . Stationarity with respect to the Lagrange multiplier, $\partial W/\partial\lambda = 0$, enforces the constraint,

$$\sum_{\sigma} \int w^\sigma(\mathbf{r}) n^\sigma(\mathbf{r}) d^3\mathbf{r} = C . \quad (3)$$

The choice of the constrained target quantity C depends on the physical property we aim to control.

In the case of constraining $\langle\hat{S}^2\rangle$, the corresponding Lagrangian can be cast as

$$W[n^\alpha, n^\beta, \lambda] = E_{\text{DFT}}[n^\alpha, n^\beta] + \lambda \left(\langle\hat{S}^2\rangle - S_c^2 \right) , \quad (4)$$

where S_c^2 is the spin-square target value. Although CDFT typically requires the constrained quantities to be expressed as explicit functionals of n^σ , as in Eq. 2, this is not possible in practice for two-electron operators such as $\langle\hat{S}^2\rangle$ since the functional form $\langle\hat{S}^2\rangle[n^\sigma]$ is unknown. A formal caveat is that $\langle\hat{S}^2\rangle$ is not rigorously defined as an exact density functional in DFT since the Kohn–Sham determinant is only an auxiliary object used to construct the density. As a result, in practical DFT calculations, $\langle\hat{S}^2\rangle$ is evaluated using the spin-resolved one-particle reduced density matrices (1-RDM). Expressed in an atomic orbital basis, the matrix element of the 1-RDM can be written as

$$P_{\mu\nu}^\sigma = \sum_{i \in \sigma} f_i^\sigma C_{\mu i}^\sigma C_{\nu i}^{\sigma*} , \quad (5)$$

where $C_{\nu i}^\sigma$ are the molecular orbital coefficients, and f_i^σ the occupations.

While n^σ can be evaluated from the spin-resolved density matrices \mathbf{P}^σ and the basis functions, the inverse mapping, from n^σ to a unique \mathbf{P}^σ , is not well-defined. This results in the unknown form of the $\delta\langle\hat{S}^2\rangle/\delta n^\sigma$ functional derivative in the the Lagrangian minimization. However, in GKS, the minimization is performed varying the 1-RDM, so we can circumvent this problem using the derivative of $\langle\hat{S}^2\rangle$ with respect to the 1-RDM, which is well-defined in the finite basis used and readily accessible throughout the SCF cycle. With this, the average spin-squared value can be incorporated into the constrained DFT framework by applying the constraint directly on $\langle\hat{S}^2[\mathbf{P}^\alpha, \mathbf{P}^\beta]\rangle$, enabling the variational minimization of the GKS energy.^{28,29}

To minimize the Lagrangian for a fixed value of λ , it is convenient to define an effective GKS Hamiltonian that incorporates the constrain as the derivative of the Lagrangian with

respect to \mathbf{P}^σ ,⁴⁰

$$F_{\mu\nu}^{c,\sigma} = \frac{d}{dP_{\mu\nu}^\sigma} W[n^\alpha, n^\beta, \lambda] \quad (6)$$

$$= F_{\mu\nu}^\sigma + \lambda \frac{d}{dP_{\mu\nu}^\sigma} \langle \hat{S}^2 \rangle, \quad (7)$$

with these effective GKS Hamiltonian matrices \mathbf{F}^σ replacing the standard KS Hamiltonian. In order to evaluate the contribution of the constraint to the \mathbf{F}^σ matrices, it is necessary to express $\langle \hat{S}^2 \rangle$ explicitly in terms of the spin-resolved density matrices,

$$\langle \hat{S}^2 \rangle = S_z(S_z + 1) + N_\beta - \sum_{\mu\nu\kappa\lambda} P_{\mu\nu}^\alpha O_{\nu\kappa} P_{\kappa\lambda}^\beta O_{\lambda\mu}, \quad (8)$$

where $S_z = (N_\alpha - N_\beta)/2$, $N_\sigma = \sum_\mu P_{\mu\nu}^\sigma O_{\nu\mu}$, and O is the standard atomic orbital overlap matrix. This expression is general for any number of unpaired electrons in monodeterminantal methods such as Hartree Fock and DFT. The spin-contamination contribution vanishes when $N_\beta = \sum_{\mu\nu\kappa\lambda} P_{\mu\nu}^\alpha O_{\nu\kappa} P_{\kappa\lambda}^\beta O_{\lambda\mu}$; a convenient set of conditions under which this equality holds is discussed and proved in Appendix B. We introduce the derivatives of Eq. 8:

$$\frac{\partial \langle \hat{S}^2 \rangle}{\partial P_{\mu\nu}^\alpha} = \frac{1}{2} (N_\alpha - N_\beta + 1) O_{\nu\mu} - [\mathbf{O} \mathbf{P}^\beta \mathbf{O}]_{\nu\mu}, \quad (9)$$

and

$$\frac{\partial \langle \hat{S}^2 \rangle}{\partial P_{\mu\nu}^\beta} = \frac{1}{2} (N_\beta - N_\alpha + 1) O_{\nu\mu} - [\mathbf{O} \mathbf{P}^\alpha \mathbf{O}]_{\mu\nu}. \quad (10)$$

We note that previous constrain approaches focused on suppressing the spin-contamination term, $N_\beta - \sum_{\mu\nu\kappa\lambda} P_{\mu\nu}^\alpha O_{\nu\kappa} P_{\kappa\lambda}^\beta O_{\lambda\mu}$, in Eq. 8. Such approach does not allow direct access to BS states with a prescribed total spin.^{29,30} In contrast, by constraining the full expectation value $\langle \hat{S}^2 \rangle$, our approach enables us, for example, to explicit target the BS singlet state with an arbitrary $\langle \hat{S}^2 \rangle$ value.

Finally, the constrained solution corresponds to a stationary point of the Lagrangian $W[n^\alpha, n^\beta, \lambda]$ with respect to both the spin-resolved density matrices \mathbf{P}^σ and the Lagrange multiplier λ . In practice, the electronic structure is optimized self-consistently using the modified GKS matrices, while λ is adjusted (in an outer loop) until the target condition $\langle \hat{S}^2 \rangle = S_c^2$ is satisfied; the specific optimization strategy and convergence thresholds are given at the end of this section.

Having established the self-consistent procedure for enforcing a target $\langle \hat{S}^2 \rangle$, we now turn to its application in the context of magnetic interactions. In particular, we use the constrained formalism to compute isotropic magnetic exchange coupling J , which for the case

two centers A and B is defined through the effective Heisenberg spin Hamiltonian^{41,42},

$$\hat{H} = -2J \hat{\mathbf{S}}_A \cdot \hat{\mathbf{S}}_B, \quad (11)$$

where $\hat{\mathbf{S}}_A$ and $\hat{\mathbf{S}}_B$ are spin operators. For comparison, we compute the exchange coupling constant J using three established schemes commonly employed in BS DFT. These expressions estimate J from the energy difference between a LS state and a HS state, where LS configuration is approximated by a BS solution and the HS configuration by a spin-pure HS reference. Each scheme relies on distinct assumptions regarding the spin character of these states and their mapping onto the effective Heisenberg Hamiltonian.

We first apply our CDFT approach using Noodleman’s expression⁴³,

$$J_N = \frac{E^{\text{BS}} - E^{\text{HS}}}{S_{\text{max}}^2}. \quad (12)$$

This expression is derived from a spin-projection argument and is formally valid in the weak-overlap limit between the magnetic orbitals. It assumes that the BS solution can be approximated as an equal-weight linear combination of the HS and LS eigenstates. Within this framework, the energy difference is rescaled by the maximum spin eigenvalue S_{max} to recover an effective exchange coupling constant. In the present work, the target $\langle \hat{S}^2 \rangle$ values used for the BS solutions are chosen to match the spin mixing assumed in Noodleman’s BS-to-Heisenberg mapping. A necessary clarification is that the spin-squared constraint is also applied to the nominally spin-pure HS state, as practical DFT calculations generally exhibit small but nonzero deviations from the ideal $\langle \hat{S}^2 \rangle$ value.

In addition to Noodleman’s formulation, we also evaluate the exchange coupling constant using two alternative schemes commonly employed in BS DFT. The second scheme, due to Ruiz and co-workers²³, is a non-projected approach designed for the strong coupling limit:

$$J_R = \frac{E^{\text{BS}} - E^{\text{HS}}}{S_{\text{max}}(S_{\text{max}} + 1)}. \quad (13)$$

Here, the BS solution is treated as a good approximation to the LS state itself, without attempting to correct for spin contamination. This approach is widely used in the literature, especially when the BS and LS states are close in character.

The third scheme is Yamaguchi’s approach,⁴⁴ also known as generalized spin-projected, which introduces a more flexible, generalized spin-projected expression:

$$J_Y = \frac{E^{\text{BS}} - E^{\text{HS}}}{\langle \hat{S}^2 \rangle_{\text{HS}} - \langle \hat{S}^2 \rangle_{\text{BS}}}. \quad (14)$$

This method accounts for spin contamination by using the expectation values of the spin-squared operator in the mapping scheme. It interpolates between the weak and strong coupling regimes, making it particularly suited for systems where the degree of spin contamination varies significantly. In the present work, only Noodleman’s approach is considered in combination with the $\langle \hat{S}^2 \rangle$ constraint, and the remaining approaches are used with unconstrained DFT solely for comparison. This restriction is motivated by conceptual consistency: Ruiz’s scheme assumes strong coupling where the BS state approximates the LS state directly, without the equal-weight mixing assumed in Noodleman’s formalism. For Yamaguchi’s scheme, applying the constraint would be redundant since enforcing the target $\langle \hat{S}^2 \rangle$ values causes its denominator to reduce to S_{max}^2 , recovering Noodleman’s expression. Thus, these unconstrained schemes serve as benchmarks for assessing how standard DFT deviations from ideal spin mixing affect J across different theoretical frameworks.

Calculations were performed using the Python-based PySCF package^{45,46}. Two model systems were considered initially: the linear triatomic molecule H_2He and the equilateral H_3He_3 cluster. For both systems, we employed the 6-311G** basis set.⁴⁷ To assess the method on a more realistic system, we also studied the bis(μ -hydroxo) Cu(II) complex. For this case, atomic coordinates were taken from Ref. 48, and for comparison with previous studies the def2-TZVP basis set⁴⁹ was used. All calculations were carried out within the unrestricted KS (UKS) framework. For the H_2He and H_3He_3 systems, we employed the PBE⁵⁰, BLYP⁵¹, PBEh⁵², B3LYP⁵³ and SCAN⁵⁴ approximate exchange-correlation functionals, representing generalized gradient approximation (GGA), hybrid, and meta-generalized gradient approximation (meta-GGA) families, respectively. For each system and functional, both the HS and BS solutions were obtained. The HS state was generated by initializing all unpaired electrons with parallel spins. The BS solution was then obtained by performing a single spin flip on one of the unpaired electrons to generate an initial guess and allowing the calculation to converge to the corresponding antiferromagnetic BS configuration.

The Lagrange multiplier λ was optimized using the Broyden-Fletcher-Goldfarb-Shanno (BFGS) quasi-Newton method⁵⁵ as implemented in `scipy.optimize.minimize`, with analytical gradients supplied to accelerate convergence (Eq. 9 and Eq. 10). The SCF convergence thresholds were set to 10^{-10} Hartree for the total energy. After SCF convergence at fixed λ , the value of $\langle \hat{S}^2 \rangle$ was evaluated and compared to the target S_c^2 . The Lagrange multiplier was then updated using the BFGS optimizer until the constraint condition was satisfied,

with the absolute deviation $|\langle \hat{S}^2 \rangle - S_c^2|$ below 10^{-5} . This outer-loop structure allows the electronic degrees of freedom and the Lagrange multiplier to be optimized in a decoupled and numerically stable manner. A more detailed discussion of the dependence of the total energy and $\langle \hat{S}^2 \rangle$ on λ , and of the qualitatively different behavior observed for HS and BS states, is provided in Appendix A.

III. RESULTS

In this section, we present J couplings obtained from both unconstrained GKS calculations and the spin-constrained CDFE approach introduced in Section II. The unconstrained results are analyzed using the three schemes described in the previous Section, and given by Eqs. 12, 13, and 14, respectively. These values are compared with the exchange coupling constant obtained from the constrained approach, J_c , which is evaluated using Noodleman's expression, Eq. 12, with spin-constrained energies for both the HS and LS states.

This systematic comparison enables an assessment of how the constraint influences the magnitude, functional dependence, and physical consistency of the computed magnetic couplings across different couplings schemes.



FIG. 1: Schematic representations of the two prototypical models considered: the linear H_2He molecule (left), for which the He–H bond distance is systematically varied (1.25, 1.625, and 2.00 Å), and the equilateral H_3He_3 cluster (right), with a fixed side length of 3.25 Å.

H₂He

We first consider the linear H₂He model system, in which the two terminal hydrogen atoms act as magnetic centers coupled through a closed-shell helium bridge, Fig. 1(a). To probe the distance dependence of the exchange interaction, three symmetric geometries were studied with He–H bond lengths of 1.25, 1.625, and 2.00 Å. The HS reference closely corresponds to the triplet state ($S = 1$), whereas the LS configuration is a BS singlet ($S = 0$), which may exhibit spin contamination in unconstrained calculations and is therefore the main target of the $\langle \hat{S}^2 \rangle$ constraint.

Tables I–III report J_N , J_R , J_Y and J_c (in cm⁻¹) for the H₂He molecule at three different He–H bond distances. At the shortest distance (1.25 Å), the system lies in the strong coupling regime, where the magnetic centers interact through significant orbital overlap. In this case, the unconstrained BS states exhibit the largest deviation of $\langle \hat{S}^2 \rangle$ with respect to the ideal value of 1, as shown in the third column of Table I. As a consequence, enforcing the constraint on $\langle \hat{S}^2 \rangle$ leads to substantial reductions in the computed J . The effect is especially evident relative to the conventional DFT schemes J_N and J_Y , for which the spin-projection factor enters explicitly through the denominator of Eqs. 12 and 14.

Ruiz’s formula performs better in this regime, since the assumptions underlying its formulation explicitly account for a strong overlap between the magnetic-center orbitals. It is important to remark that unconstrained DFT systematically overestimates the exchange coupling strength in this regime. Although the constrained values J_c are considerably smaller than their unconstrained counterparts, they remain significantly smaller than and substantially depart from the values obtained from Full-CI. At intermediate distances (1.625 Å), both the magnetic coupling strength and the degree of spin contamination are reduced. In this regime, the singlet state acquires an increasing multiconfigurational character, making the constraint applied to the BS solution more physically justified and, therefore, central to the objective of our approach. At this distance, the energy differences between the unconstrained KS-DFT calculations and the constrained approach are noticeably smaller than those observed in the short-distance regime discussed above. Although CDFT still leads to a reduction of the computed J_c , the relative impact of the constraint is less pronounced. As shown in Table II, the $\langle \hat{S}^2 \rangle$ values associated with the BS state are significantly closer to the ideal value of 1. The $\langle \hat{S}^2 \rangle$ value for the HS state continues to exhibit only a small

TABLE I: J_N , J_R , and J_Y (in cm^{-1}) for the H_2He system at a He–H bond distance of 1.25 Å.

Functional	$\langle \hat{S}^2 \rangle_{\text{HS}}$	$\langle \hat{S}^2 \rangle_{\text{BS}}$	J_N	J_R	J_Y	J_c	Full-CI ^a
PBE	2.00094	0.68264	-4567	-2283	-3465	-830	-2430
BLYP	2.00101	0.58507	-5391	-2695	-3807	-925	
PBEh	2.00098	0.81892	-3647	-1823	-3085	-792	
B3LYP	2.00105	0.74330	-4366	-2183	-3471	-863	
SCAN	2.00122	0.76966	-4333	-2166	-3520	-861	

^a Taken from Ref. 44

degree of spin contamination and shows no significant dependence on the bond length when compared to the short-distance case. At the longest distance (2.00 Å), Table III, the H

TABLE II: J_N , J_R , and J_Y (in cm^{-1}) for the H_2He system at a He–H bond distance of 1.625 Å.

Functional	$\langle \hat{S}^2 \rangle_{\text{HS}}$	$\langle \hat{S}^2 \rangle_{\text{BS}}$	J_N	J_R	J_Y	J_c	Full-CI ^a
PBE	2.00035	0.97727	-472	-236	-461	-170	-272
BLYP	2.00043	0.96355	-621	-310	-599	-217	
PBEh	2.00035	0.98488	-390	-195	-384	-159	
B3LYP	2.00043	0.97589	-512	-256	-500	-196	
SCAN	2.00047	0.97697	-474	-237	-463	-165	

^a Taken from Ref. 44

atoms are only weakly coupled through the He bridge. In this weak overlap regime, the BS solution exhibits an increased degree of spin contamination; the $\langle \hat{S}^2 \rangle$ value of the BS state is even closer to 1. As a result, the energy corrections introduced by the constraint are small. In this regime, Yamaguchi’s formula effectively reduces to Noodleman’s expression. Since the latter assumes a maximally multiconfigurational character in the weak-coupling limit, this behavior is naturally captured by Yamaguchi’s scheme, as reflected by the very similar

values of the J_N and J_Y in columns 4 and 6, respectively. Figure 2, in panels a, b and c,

TABLE III: J_N , J_R , and J_Y (in cm^{-1}) for the H_2He system at a He–H bond distance of 2.0 Å.

Functional	$\langle \hat{S}^2 \rangle_{\text{HS}}$	$\langle \hat{S}^2 \rangle_{\text{BS}}$	J_N	J_R	J_Y	J_c	Full-CI ^a
PBE	2.00008	0.99824	-45	-22	-45	-25	-25
BLYP	2.00014	0.99675	-69	-34	-69	-42	
PBEh	2.00008	0.99878	-37	-18	-37	-23	
B3LYP	2.00013	0.99770	-56	-28	-56	-35	
SCAN	2.00014	0.99828	-39	-19	-39	-24	

^a Taken from Ref. 44

provides a graphical representation of the J reported in Tables I–III for the H_2He system at the three He–H bond distances considered. Dotted lines denote values of J obtained from unconstrained DFT calculations, while the continuous lines correspond to results obtained using the spin-constrained DFT formalism. These lines connecting the different dots are included as a guide to the eye to emphasize trends across different exchange–correlation functionals. At 1.25 and 1.625 Å, the constrained calculations yield exchange-coupling constants that are less sensitive to the choice of exchange–correlation functional. This reduction in functional dependence is particularly evident when compared to the broader dispersion observed in the unconstrained DFT results. In addition, the constrained J values are systematically smaller in magnitude, as expected given the commonly reported overestimation of magnetic exchange interactions by standard BS-DFT. In Fig. 2c, the values corresponding to the Yamaguchi formula and the Noodleman formula coincide. Overall, Fig. 2 demonstrates that enforcing the $\langle \hat{S}^2 \rangle$ constraint not only lowers the magnitude of the J but also stabilizes their functional dependence. This increased consistency supports the interpretation that the constrained framework yields more physically meaningful and transferable estimates of magnetic exchange interactions than unconstrained BS-DFT.

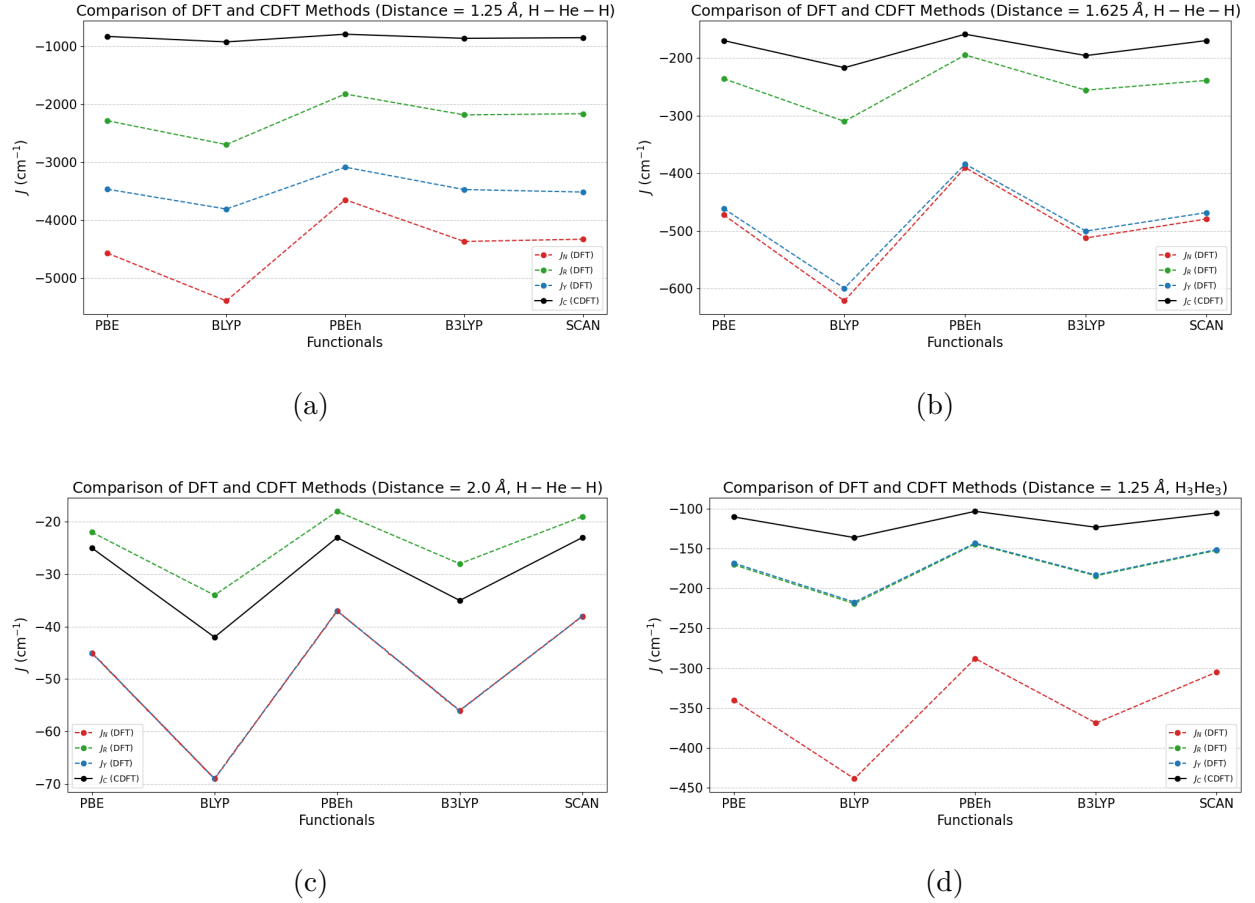


FIG. 2: Dependence of the total energy and the spin-squared expectation value $\langle \hat{S}^2 \rangle$ on the Lagrange multiplier λ for the H_2He system at three different He–H bond distances. And, on the bottom right, for the triangular H_3He_3

H_3He_3

We next consider the triangular H_3He_3 cluster shown in Fig. 1(b), which introduces a multi-center coupling topology absent in the linear H_2He model. The three hydrogen atoms occupy the vertices of an equilateral triangle with side length 3.25 Å, while the three helium atoms are located at the midpoints of each edge, resulting in a fixed H–He distance of 1.625 Å. The HS reference corresponds to a quartet state ($S = 3/2$), whereas the LS configuration is described by a doublet ($S = 1/2$). As in the linear case, the BS solution may exhibit spin contamination. Accordingly, we apply the $\langle \hat{S}^2 \rangle$ constraint to enforce a target value of 1.75, corresponding to an equal admixture of a doublet and a quartet. The triangular geometry introduces competing magnetic interactions between the three hydrogen centers, which can

give rise to spin frustration, i.e., a situation in which not all pairwise spin couplings can be simultaneously optimized. This geometric constraint is therefore expected to weaken the effective magnetic coupling relative to the linear H₂He system.

Table IV shows exchange couplings obtained from unconstrained DFT calculations, and the constrained value J_c computed within the CDFT framework. Consistent with the behavior observed for the linear system, imposing the spin-squared constraint systematically reduces the magnitude of the exchange coupling constants across all functionals. The values

TABLE IV: J_N , J_R , and J_Y (in cm⁻¹) for the H₃He₃ system at a He–H bond distance of 1.625 Å.

Functional	$\langle \hat{S}^2 \rangle_{\text{HS}}$	$\langle \hat{S}^2 \rangle_{\text{BS}}$	J_N	J_R	J_Y	J_c	CASPT2 ^a
PBE	3.75079	1.73277	-340	-170	-168	-110	-195
BLYP	3.75087	1.72537	-439	-219	-217	-136	
PBEh	3.75073	1.73827	-288	-144	-143	-103	
B3LYP	3.75082	1.73287	-369	-184	-183	-123	
SCAN	3.75091	1.73396	-305	-152	-151	-105	

^a Taken from Ref. 4

of $\langle \hat{S}^2 \rangle$ obtained for the HS state are very close to the expected value of 3.75, reflecting its nearly spin-pure character. As a result, enforcing the constraint to recover the exact value of $\langle \hat{S}^2 \rangle = 3.75$ leads to only minor corrections to the HS energies, which nevertheless contribute to the evaluation of the constrained exchange coupling constant J_c . In contrast, the BS solutions exhibit larger deviations from the ideal target value of 1.75. With the exception of BLYP, which yields slightly lower $\langle \hat{S}^2 \rangle$ values, the BS spin expectation values are similar across the different functionals. Despite this variation, the resulting constrained exchange couplings J_c are comparable for all functionals.

When compared to the linear H₂He system at a similar bond-lengths, the absolute values of the J for H₃He₃ are smaller. This reduction is consistent with a weakened effective magnetic coupling arising from spin frustration and a more delocalized distribution of the spin density over the triangular cluster.

Bis(μ -hydroxo) Cu(II)

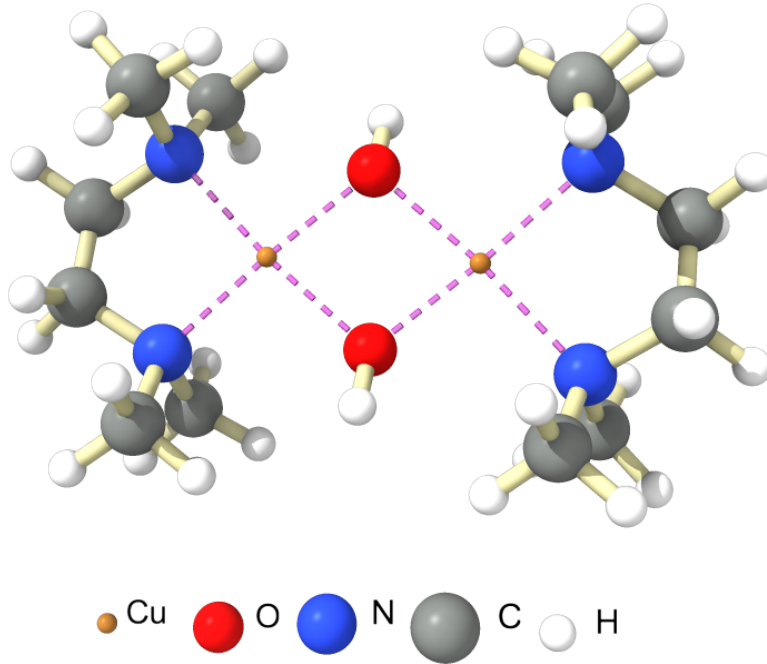
As a realistic test case, we finally examine the bis(μ -hydroxo) Cu(II) complex (Fig. 3). This complex carries a total charge of 2 and is treated in two spin configurations: a triplet HS state ($S = 1$) and a LS singlet state ($S = 0$) modeled via a BS solution with antiferromagnetically aligned local moments on the two Cu(II) centers. The two copper atoms are separated by approximately 2.97 Å, and the magnetic interaction is mediated by bridging ligands (oxygen donors) in a non-collinear geometry, giving rise to a more delocalized and angle-dependent superexchange pathway than in the linear H₂He model. Due to the partially filled Cu d -manifold and the multireference character of the singlet, the BS state can exhibit substantial spin contamination. We therefore apply the constraint to enforce the target spin character of the BS state ($\langle \hat{S}^2 \rangle = 1$) and assess its impact on the computed exchange couplings. Table V shows the calculated magnetic exchange couplings for the bis(μ -hydroxo) Cu(II) complex. The values of $\langle \hat{S}^2 \rangle$ obtained for the HS state are very close to the ideal spin-pure value, indicating minimal spin contamination. In contrast, the BS solutions exhibit substantial deviations from the ideal value of $\langle \hat{S}^2 \rangle = 1$, with the exception of the two hybrid functionals employed, PBEh and B3LYP, for which the BS spin expectation values are already close to 1. For the BLYP and PBE functionals, the application of the spin-squared constraint leads to a systematic reduction in the magnitude of the exchange coupling constants, consistent with the trends observed for the simpler H₂He and H₃He₃ systems. This behavior reflects the energetic penalty imposed by the constraint on the spin-contaminated BS state, which increases the BS energy relative to the HS reference and consequently lowers the resulting exchange coupling. In contrast to the local and semi-local functionals, the

TABLE V: J_N , J_R , and J_Y (in cm⁻¹) for the bis(μ -hydroxo) Cu(II) complex.

Functional	$\langle \hat{S}^2 \rangle_{\text{HS}}$	$\langle \hat{S}^2 \rangle_{\text{BS}}$	J_N	J_R	J_Y	J_c	Experimental ^a
BLYP	2.00293	0.80620	-743	-371	-621	-342	-180
PBE	2.00299	0.81101	-729	-364	-612	-342	
PBEh	2.00646	0.98751	-167	-83	-164	-724	
B3LYP	2.00559	0.97732	-225	-112	-219	-638	

^a Taken from Ref. 48

FIG. 3: Molecular structure of the bis(μ -hydroxo) Cu(II) complex with bridging hydroxo ligands. The Cu–Cu distance of 2.97 Å and the Cu–O–Cu angle give rise to an angle-dependent superexchange pathway.



hybrid functionals PBEh and B3LYP exhibit a qualitatively different response to the spin-squared constraint. In this case, the constrained J_c increases in magnitude. This indicates that, for hybrid functionals, the application of the constraint modifies the energetic balance between the HS and BS states in a manner distinct from that observed for semi-local approximations. This behavior can be rationalized by considering the electronic structure of the BS state obtained with hybrid functionals. In general, the spin-squared constraint has a larger energetic impact on the BS solution than on the HS reference, increasing the BS energy and thereby reducing the HS–BS energy gap and the resulting exchange coupling constant. However, hybrid functionals partially correct self-interaction errors and promote stronger localization of the spin density, yielding BS solutions that are intrinsically closer to the symmetry-broken limit. As reflected by the $\langle \hat{S}^2 \rangle$ values reported in the third column

of Table V, the unconstrained BS states obtained with hybrid functionals are already close to the ideal value of 1. Consequently, the additional constraint has a comparatively small effect on the BS energy than on the HS energy. The net effect is an increase in the HS–BS energy gap, which leads to larger values of the exchange coupling constant. This mechanism is illustrated by the marked difference between the unconstrained BS spin expectation values obtained with BLYP ($\langle \hat{S}^2 \rangle \approx 0.80$) and those obtained with B3LYP ($\langle \hat{S}^2 \rangle \approx 0.97$), the latter being much closer to the ideal BS value. This trend was not observed in the H₂He and H₃He₃ molecules.

Overall, the bis(μ -hydroxo) Cu(II) results demonstrate that the spin-squared constraint is an effective tool for correcting the systematic overestimation of exchange interactions in local and semi-local density functionals. For hybrid functionals, however, the constraint must be applied with care, as the improved treatment of self-interaction and enhanced spin localization fundamentally alter the balance between spin contamination, energetic penalties, and magnetic coupling.

IV. CONCLUSIONS

In this work, we formulated a constrained DFT approach within the GKS framework that enables explicit control of $\langle \hat{S}^2 \rangle$ through a Lagrange multiplier. Rather than eliminating spin contamination in BS solutions, the method enforces physically motivated spin mixing consistent with BS-based exchange-coupling models. For example, the target values $\langle \hat{S}^2 \rangle = 1$ (singlet–triplet) and $\langle \hat{S}^2 \rangle = 1.75$ (doublet–quartet) are recovered by construction. We also derived analytical gradients of $\langle \hat{S}^2 \rangle$ with respect to spin-resolved density matrices, enabling an efficient SCF implementation. These expressions are general for arbitrary spin manifolds and do not rely on a specific exchange-correlation functional, providing a practical route for constrained BS calculations across different chemical systems.

Applied to H₂He, H₃He₃, and the bis(μ -hydroxo) Cu(II) complex exchange couplings, the constraint reduces functional-dependent variability in calculated J couplings and stabilizes the spin character of BS solutions. The constrained J values are generally smaller in magnitude than unconstrained ones, particularly for semi-local functionals, where spin contamination is more pronounced. An exception is the bis(μ -hydroxo) Cu(II) complex with hybrid functionals (PBEh, B3LYP), where unconstrained BS solutions are already close to

$\langle \hat{S}^2 \rangle \approx 1$, and the constraint can increase $|J|$ through a stronger impact on the HS reference.

V. ACKNOWLEDGMENTS

This work was supported by the U.S. Department of Energy, Office of Science, Office of Basic Energy Sciences, as part of the Computational Chemical Sciences Program under Award No. DE-SC0005027.

Appendix A: The effect of λ

To clarify the role of the Lagrange multiplier in the spin-squared constrained formalism, we examine how both the total energy and $\langle \hat{S}^2 \rangle$ change as λ is varied. Figure 4 summarizes this dependence for HS and BS solutions in H_2He and the bis(μ -hydroxo) Cu(II) complex, allowing a direct comparison of the constraint’s impact on the two spin manifolds. As shown below, the response is qualitatively different in the HS and BS cases, which has important consequences for how λ should be chosen and optimized in practical calculations. For the HS state in the H_2He molecule and the bis(μ -hydroxo) Cu(II) complex (Figs. 4a and 4c respectively), both the total energy and $\langle \hat{S}^2 \rangle$ exhibit a smooth and monotonic dependence on the Lagrange multiplier λ . As $\lambda \rightarrow \infty$, both quantities approach well-defined asymptotic limits, reflecting the progressive elimination of residual spin contamination in the HS solution. This behavior indicates that an explicit optimization of the constrained Lagrangian with respect to λ is not required for the HS state: selecting a sufficiently large multiplier is sufficient to recover a spin-pure reference. Although spin contamination in HS states is typically small, the calculation of J is highly sensitive to even minor deviations in $\langle \hat{S}^2 \rangle$, making HS spin decontamination advisable.

Insight into this behavior can be obtained by examining Eq. 8. The spin-contamination contribution vanishes when the condition

$$N_\beta = \sum_{\mu\nu\kappa\lambda} P_{\mu\nu}^\alpha O_{\nu\kappa} P_{\kappa\lambda}^\beta O_{\lambda\mu} \quad (\text{A1})$$

is satisfied. The trace on the right-hand side can be rewritten as

$$\sum_{i=1}^{N_\alpha} \sum_{j=1}^{N_\beta} \left| \langle \phi_i^\alpha | \phi_j^\beta \rangle \right|^2, \quad (\text{A2})$$

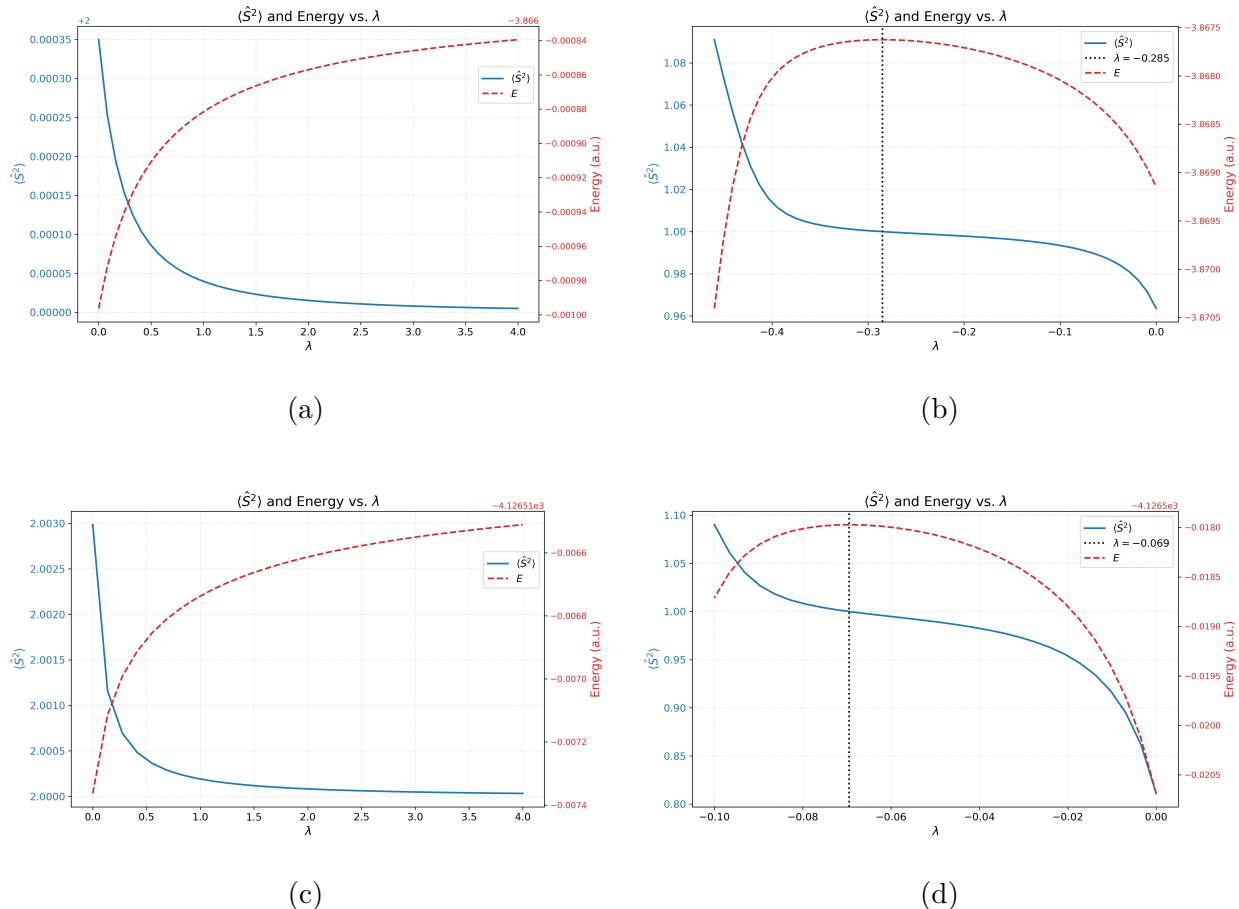


FIG. 4: Total energy and $\langle \hat{S}^2 \rangle$ as functions of λ for HS (left) and BS (right) states in H_2He (top) and the bis(μ -hydroxo) Cu(II) complex (bottom). HS curves are monotonic, while BS curves show a stationary point.

which might suggest that Eq. A1 holds only when the occupied α and β orbitals are identical. This interpretation would imply that complete orbital pairing is required to eliminate spin contamination.

A closely related constraint was previously introduced by Andrews et al.,²⁹ within the Hartree–Fock framework, where the restriction was imposed directly on the trace term in Eq. 8. They demonstrated that, in the limit $\lambda \rightarrow \infty$, restricted open-shell Hartree–Fock solutions are obtained. While this result is consistent with the interpretation above, the present analysis shows that Eq. A1 does not require such a strong condition. In particular, the equality holds whenever the occupied β manifold can be expressed as linear combinations of the occupied α orbitals, without requiring one-to-one orbital pairing. A formal proof of this result is provided in Appendix B.

In contrast, the BS solution for the H₂He molecule (Fig. 4b) and for the bis(μ -hydroxo) Cu(II) complex (Fig. 4d) displays a qualitatively different behavior. Both the energy and $\langle \hat{S}^2 \rangle$ exhibit a stationary point as functions of λ , making an explicit optimization with respect to the Lagrange multiplier necessary. Performing the optimization of the Lagrangian with respect to λ in H₂He yields a stationary point at $\lambda \approx -0.28$, indicated by the vertical dashed line in Fig. 4. In the case of the bis(μ -hydroxo) Cu(II) complex, the maximum point is at $\lambda \approx -0.07$. These stationary points correspond to a maximum of the constrained energy, reflecting the fact that the constraint penalizes deviations from the target spin value. At this optimal λ , the BS solution satisfies the imposed condition $\langle \hat{S}^2 \rangle = 1$ exactly, providing a consistent and well-defined low-spin reference for the evaluation of J .

Appendix B: Conditions for $\text{Tr}(\mathbf{P}^\alpha \mathbf{P}^\beta) = N_\beta$

Consider Eq. 8 and, for clarity, let us work on an orthonormal basis. In this case, the overlap matrix reduces to the identity and the expectation value of \hat{S}^2 can be written as

$$\langle \hat{S}^2 \rangle = S_z(S_z + 1) + N_\beta - \sum_{\mu\nu} P_{\mu\nu}^\alpha P_{\nu\mu}^\beta \quad (\text{B1})$$

$$= S_z(S_z + 1) + N_\beta - \text{Tr}(\mathbf{P}^\alpha \mathbf{P}^\beta). \quad (\text{B2})$$

Since the trace is invariant under unitary transformations, the following derivation is fully equivalent to the general expression in Eq. 8 written in a nonorthogonal atomic-orbital basis.

The spin-resolved density matrices can be expressed as projectors onto the subspaces spanned by the occupied spatial orbitals of each spin,

$$\mathbf{P}^\alpha = \sum_{i=1}^{N_\alpha} |\phi_i^\alpha\rangle \langle \phi_i^\alpha|, \quad (\text{B3})$$

$$\mathbf{P}^\beta = \sum_{j=1}^{N_\beta} |\phi_j^\beta\rangle \langle \phi_j^\beta|, \quad (\text{B4})$$

where $\{\phi_i^\alpha\}$ and $\{\phi_j^\beta\}$ denote orthonormal sets of occupied spatial orbitals.

Using these definitions, it is straightforward to show that

$$\text{Tr}(\mathbf{P}^\alpha \mathbf{P}^\beta) = \sum_{i=1}^{N_\alpha} \sum_{j=1}^{N_\beta} \left| \langle \phi_i^\alpha | \phi_j^\beta \rangle \right|^2, \quad (\text{B5})$$

which depends only on the mutual overlaps between the occupied α and β spatial orbitals.

Introducing the overlap matrix between the two orbital sets,

$$O_{ij} = \langle \phi_i^\alpha | \phi_j^\beta \rangle, \quad (\text{B6})$$

Eq. (B5) can be written in compact form as

$$\text{Tr}(\mathbf{P}^\alpha \mathbf{P}^\beta) = \text{Tr}(\mathbf{O}^\dagger \mathbf{O}). \quad (\text{B7})$$

We now assume that the occupied β orbitals are contained in the subspace spanned by the occupied α orbitals, such that each β orbital can be expressed as a linear combination of the α orbitals,

$$|\phi_j^\beta\rangle = \sum_{i=1}^{N_\alpha} C_{ij} |\phi_i^\alpha\rangle. \quad (\text{B8})$$

This condition reflects a geometric inclusion of subspaces and does not imply equality or pairing of individual α and β orbitals.

Using the orthonormality of the α orbitals, the orthonormality of the β orbitals implies

$$\delta_{jj'} = \langle \phi_j^\beta | \phi_{j'}^\beta \rangle \quad (\text{B9})$$

$$= \sum_{i,i'} C_{ij}^* C_{i'j'} \langle \phi_i^\alpha | \phi_{i'}^\alpha \rangle \quad (\text{B10})$$

$$= \sum_i C_{ij}^* C_{ij'}, \quad (\text{B11})$$

which, in matrix form, yields

$$\mathbf{C}^\dagger \mathbf{C} = \mathbf{1}_{N_\beta}. \quad (\text{B12})$$

Substituting Eq. (B8) into the definition of the overlap matrix,

$$O_{ij} = \langle \phi_i^\alpha | \phi_j^\beta \rangle \quad (\text{B13})$$

$$= \sum_{k=1}^{N_\alpha} C_{kj} \langle \phi_i^\alpha | \phi_k^\alpha \rangle \quad (\text{B14})$$

$$= C_{ij}, \quad (\text{B15})$$

so that $\mathbf{O} = \mathbf{C}$. Consequently,

$$\text{Tr}(\mathbf{O}^\dagger \mathbf{O}) = \text{Tr}(\mathbf{C}^\dagger \mathbf{C}) = \text{Tr}(\mathbf{1}_{N_\beta}) = N_\beta. \quad (\text{B16})$$

Therefore, when the occupied β manifold are entirely contained within the subspace spanned by the occupied α orbitals, the trace term in Eq. 8 equals the number of β electrons. In this case, the additional contribution to $\langle \hat{S}^2 \rangle$ vanishes and the Slater determinant is an eigenfunction of \hat{S}^2 , yielding the correct spin value without spin contamination.

REFERENCES

- ¹P. Hohenberg and W. Kohn, “Inhomogeneous electron gas,” *Phys. Rev.* **136**, B864–B871 (1964).
- ²W. Kohn and L. J. Sham, “Self-consistent equations including exchange and correlation effects,” *Phys. Rev.* **140**, A1133–A1138 (1965).
- ³K. Treppe, S. Schwalbe, S. Liebing, W. T. Schulze, J. Kortus, H. Myneni, A. V. Ivanov, and S. Lehtola, “Chemical bonding theories as guides for self-interaction corrected solutions: Multiple local minima and symmetry breaking,” *J. Chem. Phys.* **155**, 224109 (2021).
- ⁴E. Ruiz, S. Alvarez, J. Cano, and V. Polo, “About the calculation of exchange coupling constants using density-functional theory: The role of the self-interaction error,” *J. Chem. Phys.* **123**, 164110 (2005).
- ⁵P. Mori-Sánchez, A. J. Cohen, and W. Yang, “Localization and delocalization errors in density functional theory and implications for band-gap prediction,” *Phys. Rev. Lett.* **100**, 146401 (2008).
- ⁶K. R. Bryenton, A. A. Adeleke, S. G. Dale, and E. R. Johnson, “Delocalization error: The greatest outstanding challenge in density-functional theory,” *WIREs Comput. Mol. Sci.* **13**, e1631 (2023).
- ⁷E. Sim, S. Song, S. Vuckovic, and K. Burke, “Improving results by improving densities: Density-corrected density functional theory,” *J. Am. Chem. Soc.* **144**, 6625–6639 (2022).
- ⁸C. A. Gaggioli, S. J. Stoneburner, C. J. Cramer, and L. Gagliardi, “Beyond density functional theory: the multiconfigurational approach to model heterogeneous catalysis,” *ACS Catal.* **9**, 8481–8502 (2019).
- ⁹J. M. Herbert, “Density-functional theory for electronic excited states,” in *Theoretical and computational photochemistry* (Elsevier, 2023) pp. 69–118.
- ¹⁰Q. Wu and T. Van Voorhis, “Constrained density functional theory and its application in long-range electron transfer,” *J. Chem. Theory Comput.* **2**, 765–774 (2006).

- ¹¹C. Adamo and D. Jacquemin, “The calculations of excited-state properties with time-dependent density functional theory,” *Chem. Soc. Rev.* **42**, 845–856 (2013).
- ¹²T. Stein, L. Kronik, and R. Baer, “Reliable prediction of charge transfer excitations in molecular complexes using time-dependent density functional theory,” *J. Am. Chem. Soc.* **131**, 2818–2820 (2009).
- ¹³T. Gould and L. Kronik, “Ensemble generalized kohn–sham theory: The good, the bad, and the ugly,” *J. Chem. Phys.* **154** (2021).
- ¹⁴P. Dederichs, S. Blügel, R. Zeller, and H. Akai, “Ground states of constrained systems: application to cerium impurities,” *Phys. Rev. Lett.* **53**, 2512 (1984).
- ¹⁵B. Kaduk, T. Kowalczyk, and T. Van Voorhis, “Constrained density functional theory,” *Chem. Rev.* **112**, 321–370 (2012).
- ¹⁶Q. Wu and T. Van Voorhis, “Direct calculation of electron transfer parameters through constrained density functional theory,” *J. Phys. Chem. A* **110**, 9212–9218 (2006).
- ¹⁷W. Ni, X. Zhang, X. Yue, Z. Zhang, Y. Zhang, K. Wang, W. Dai, and X. Fu, “Visible light enhanced thermocatalytic reverse water gas shift reaction via localized surface plasmon resonance of copper nanoparticles,” *Sep. Purif. Technol.* **361**, 131514 (2025).
- ¹⁸J. J. Phillips and J. E. Peralta, “Magnetic exchange couplings from constrained density functional theory: An efficient approach utilizing analytic derivatives,” *J. Chem. Phys.* **135** (2011).
- ¹⁹I. Rudra, Q. Wu, and T. Van Voorhis, “Accurate magnetic exchange couplings in transition-metal complexes from constrained density-functional theory,” *J. Chem. Phys.* **124** (2006).
- ²⁰L. Fonseca, J. Jimenez, J. Leburton, and R. M. Martin, “Self-consistent electronic structure, coulomb interaction, and spin effects in self-assembled strained inas–gaas quantum dot structures,” *Physica E* **2**, 743–747 (1998).
- ²¹O. Eriksson, J. M. Wills, M. Colarieti-Tosti, S. Lebegue, and A. Grechnev, “Many-body projector orbitals for electronic structure theory of strongly correlated electrons,” *Int. J. Quantum Chem.* **105**, 160–165 (2005).
- ²²B. Hourahine, B. Aradi, and T. Frauenheim, “DFTB+ and lanthanides,” in *J. Phys.: Conf. Ser.*, Vol. 242 (IOP Publishing, 2010) p. 012005.
- ²³E. Ruiz, J. Cano, S. Alvarez, and P. Alemany, “Broken symmetry approach to calculation of exchange coupling constants for homobinuclear and heterobinuclear transition metal

- complexes,” *J. Comput. Chem.* **20**, 1391–1400 (1999).
- ²⁴H. C. Fitzhugh, J. W. Furness, M. R. Pederson, J. E. Peralta, and J. Sun, “Comparative density functional theory study of magnetic exchange couplings in dinuclear transition-metal complexes,” *J. Chem. Theory Comput.* **19**, 5760–5772 (2023).
- ²⁵K. Dema, Z. Hooshmand, and M. R. Pederson, “Electronic and magnetic signatures of low-lying spin-flip excitonic states of Mn^{2+} -acetate,” *Polyhedron* **206**, 115332 (2021).
- ²⁶N. Ferré, N. Guihéry, and J.-P. Malrieu, “Spin decontamination of broken-symmetry density functional theory calculations: deeper insight and new formulations,” *Phys. Chem. Chem. Phys.* **17**, 14375–14382 (2015).
- ²⁷G. David, G. Trinquier, and J.-P. Malrieu, “Consistent spin decontamination of broken-symmetry calculations of diradicals,” *J. Chem. Phys.* **153** (2020).
- ²⁸T. Tsuchimochi and G. E. Scuseria, “Constrained active space unrestricted mean-field methods for controlling spin-contamination,” *J. Chem. Phys.* **134** (2011).
- ²⁹J. S. Andrews, D. Jayatilaka, R. G. Bone, N. C. Handy, and R. D. Amos, “Spin contamination in single-determinant wavefunctions,” *Chem. Phys. Lett.* **183**, 423–431 (1991).
- ³⁰J. Schmidt, N. Shenvi, and J. C. Tully, “Controlling spin contamination using constrained density functional theory,” *J. Chem. Phys.* **129** (2008).
- ³¹A. A. Ovchinnikov and J. K. Labanowski, “Simple spin correction of unrestricted density-functional calculation,” *Phys. Rev. A* **53**, 3946 (1996).
- ³²I. de P.R. Moreira and F. Illas, “A unified view of the theoretical description of magnetic coupling in molecular chemistry and solid state physics,” *Phys. Chem. Chem. Phys.* **8**, 1645–1659 (2006).
- ³³P.-O. Löwdin, “Angular momentum wavefunctions constructed by projector operators,” *Rev. Mod. Phys.* **36**, 966–976 (1964).
- ³⁴P. Rivero, I. de P.R. Moreira, F. Illas, and G. E. Scuseria, “Reliability of range-separated hybrid functionals for describing magnetic coupling in molecular systems,” *J. Chem. Phys.* **129** (2008).
- ³⁵J. P. Perdew, “SCAN meta-GGA, strong correlation, symmetry breaking, self-interaction correction, and semi-classical limit in density functional theory: Hidden connections and beneficial synergies?” *APL Comput. Phys.* **1** (2025).
- ³⁶P. Mori-Sánchez, A. J. Cohen, and W. Yang, “Many-electron self-interaction error in approximate density functionals,” *J. Chem. Phys.* **125** (2006).

- ³⁷U. von Barth and L. Hedin, “A local exchange-correlation potential for the spin polarized case. I,” *J. Phys. C: Solid State Phys.* **5**, 1629 (1972).
- ³⁸J. P. Perdew and A. Zunger, “Self-interaction correction to density-functional approximations for many-electron systems,” *Phys. Rev. B* **23**, 5048–5079 (1981).
- ³⁹P. K. Chattaraj, *Spin-Polarized Density Functional Theory: Chemical Reactivity . Chemical reactivity theory: a density functional view*, edited by R. Vargas and M. Galván (CRC press, 2009).
- ⁴⁰S. Lehtola, F. Blockhuys, and C. Van Alsenoy, “An overview of self-consistent field calculations within finite basis sets,” *Molecules* **25**, 1218 (2020).
- ⁴¹R. Caballol, O. Castell, F. Illas, I. de P. R. Moreira, and J. Malrieu, “Remarks on the proper use of the broken symmetry approach to magnetic coupling,” *J. Phys. Chem. A* **101**, 7860–7866 (1997).
- ⁴²A. V. Postnikov, J. Kortus, and M. R. Pederson, “Density functional studies of molecular magnets,” *phys. Status solidi (b)* **243**, 2533–2572 (2006).
- ⁴³L. Noodleman, “Valence bond description of antiferromagnetic coupling in transition metal dimers,” *J. Chem. Phys.* **74**, 5737–5743 (1981).
- ⁴⁴T. Soda, Y. Kitagawa, T. Onishi, Y. Takano, Y. Shigeta, H. Nagao, Y. Yoshioka, and K. Yamaguchi, “Ab initio computations of effective exchange integrals for H–H, H–He–H and Mn₂O₂ complex: comparison of broken-symmetry approaches,” *Chem. Phys. Lett.* **319**, 223–230 (2000).
- ⁴⁵Q. Sun, X. Zhang, S. Banerjee, P. Bao, M. Barbry, N. S. Blunt, N. A. Bogdanov, G. H. Booth, J. Chen, Z.-H. Cui, J. J. Eriksen, Y. Gao, S. Guo, J. Hermann, M. R. Hermes, K. Koh, P. Koval, S. Lehtola, Z. Li, J. Liu, N. Mardirossian, J. D. McClain, M. Motta, B. Mussard, H. Q. Pham, A. Pulkin, W. Purwanto, P. J. Robinson, E. Ronca, E. R. Sayfutyarova, M. Scheurer, H. F. Schurkus, J. E. T. Smith, C. Sun, S.-N. Sun, S. Upadhyay, L. K. Wagner, X. Wang, A. White, J. D. Whitfield, M. J. Williamson, S. Wouters, J. Yang, J. M. Yu, T. Zhu, T. C. Berkelbach, S. Sharma, A. Y. Sokolov, and G. K.-L. Chan, “Recent developments in the pyscf program package,” *J. Chem. Phys.* **153**, 024109 (2020).
- ⁴⁶S. Lehtola, C. Steigemann, M. J. Oliveira, and M. A. Marques, “Recent developments in libxc — a comprehensive library of functionals for density functional theory,” *SoftwareX* **7**, 1–5 (2018).
- ⁴⁷R. Krishnan, J. S. Binkley, R. Seeger, and J. A. Pople, “Self-consistent molecular orbital

- methods. xx. a basis set for correlated wave functions,” J. Chem. Phys. **72**, 650–654 (1980).
- ⁴⁸G. Singh, S. Gamboa, M. Orio, D. A. Pantazis, and M. Roemelt, “Magnetic exchange coupling in cu dimers studied with modern multireference methods and broken-symmetry coupled cluster theory,” Theor. Chem. Acc. **140**, 1–15 (2021).
- ⁴⁹F. Weigend and R. Ahlrichs, “Balanced basis sets of split valence, triple zeta valence and quadruple zeta valence quality for h to rn: Design and assessment of accuracy,” Phys. Chem. Chem. Phys. **7**, 3297–3305 (2005).
- ⁵⁰J. P. Perdew, K. Burke, and M. Ernzerhof, “Generalized gradient approximation made simple,” Phys. Rev. Lett. **77**, 3865 (1996).
- ⁵¹A. D. Becke, “Density-functional exchange-energy approximation with correct asymptotic behavior,” Phys. Rev. A **38**, 3098 (1988).
- ⁵²C. Adamo and V. Barone, “Toward reliable density functional methods without adjustable parameters: The PBE0 model,” J. Chem. Phys. **110**, 6158–6170 (1999).
- ⁵³A. D. Becke, “Density-functional thermochemistry. III. The role of exact exchange,” J. Chem. Phys. **98**, 5648–5652 (1993).
- ⁵⁴J. Sun, A. Ruzsinszky, and J. P. Perdew, “Strongly constrained and appropriately normed semilocal density functional,” Phys. Rev. Lett. **115**, 036402 (2015).
- ⁵⁵J. Nocedal and S. J. Wright, *Numerical optimization* (Springer, 2006) see Section 6.1 (BFGS).